JOURNAL OF SOLID STATE CHEMISTRY 101, 322–330 (1992)

High Resolution Electron Microscopy Study of $Sr_2NdNbCu_2O_8$

H. W. ZANDBERGEN,*,[1] R. J. CAVA,† J. J. KRAJEWSKI,† AND W. F. PECK, JR.†

*National Center for High Resolution Electron Microscopy, Laboratory of Materials Science, Delft University of Technology, Rotterdamseweg 137, 2628 AL Delft, The Netherlands; and †AT&T Bell Laboratories, Murray Hill, New Jersey

Received January 27, 1992; in revised form May 11, 1992; accepted May 12, 1992

The structure of $Sr_2NdNbCu_2O_8$ (tetragonal, space group *P4bm*, $a = 0.549$, $c = 1.166$ nm) and crystallographic defects occurring therein have been studied with high resolution electron microscopy and electron diffraction. The structure of $Sr_2NdNbCu_2O_8$ consists of a layer sequence $Nd–CuO_2–SrO–NbO_2–SrO–CuO_2$ having a perovskite-like structure. This structure is very similar to that of $YBa_2Cu_3O_7$: Y is replaced by Nd and the CuO layer by a NbO_2 layer. $Sr_2NdNbCu_2O_8$ has an $a_p\sqrt{2}, a_p\sqrt{2}, c$ superstructure, due to rotation of the NbO_6 octahedra about the c-axis, leading to a space group *P4bm*. This superstructure is often short range. Intergrowths occur with an approximate composition of $Sr(Nb,Cu)O_3$, which adopts a modified simple perovskite structure. Also, examples are shown of [110] 90° rotation twins and edge dislocations. © 1992 Academic Press, Inc.

Introduction

Since the discovery of superconductivity in the $La_{2-x}Ba_xCuO_4$ system (*1*), many high-temperature copper oxide superconductors have been reported. All these superconductors are based on the presence of CuO_2 planes. The CuO_2 planes are stacked with other metal oxide layers. The structures of the copper oxide superconductors differ in the composition of the additional metal oxide layers and in the way in which these layers are stacked with each other and with the CuO_2 layers. Three types of stacking can be observed: perovskite-like, rock salt like, and fluorite-like. The perovskite structure consists of an alternate stacking of an AO layer with a BO_2 layer. The rock salt structure consists of a stacking of AO and BO layers, and the fluorite structure of a stacking of A and O_2 layers.

Recently Cava *et al.* (*2*) reported a superconducting transition temperature of 28 K for $Sr_2Nd_{1.5}Ce_{0.5}NbCu_2O_{10-\delta}$ and $Sr_2Nd_{1.5}Ce_{0.5}TaCu_2O_{10-\delta}$. The structure of $Sr_2Nd_{1.5}Ce_{0.5}NbCu_2O_{10-\delta}$ (*2, 3*) consists of a block of $CuO_2–SrO–NbO_2–SrO–CuO_2$ layers having a perovskite-like structure sandwiched with a $(Nd,Ce)–O_2–(Nd,Ce)$ block which has fluorite-like stacking. The doping of holes to the CuO_2 layers can be varied by variation of the Nd/Ce ratio. The maximum T_c is observed for the compositions $Nd_{1.5}Ce_{0.5}$ and $Nd_{1.4}Ce_{0.6}$.

A number of defects have been observed (*4*) in $Sr_2Nd_{1.5}Ce_{0.5}NbCu_2O_{10-\delta}$. The most dominant defects were those belonging to the series $Sr_2(Nd,Ce)_nNbCu_2O_{6+2n-\delta}$. De-

[1] Author to whom all correspondence should be sent.

0022-4596/92 $5.00

fects are observed in which the number of (Nd,Ce) layers varies from 1 to 5. The $n = 1$ material was found to extend over relatively larger areas. $n = 3$, $n = 4$, and $n = 5$ phases occur only as single planar defects. Apart from these defects, planar defects with a composition of $Sr(Nd,Ce)Cu_2O_5$ and intergrowths with an approximate composition of $Sr(Nb,Cu)O_3$, having the perovskite structure, are observed.

The observation of extended areas of the $n = 1$ defect prompted us to attempt to prepare it as a pure phase. These attempts were successful for the composition $Sr_2NdNbCu_2O_8$. In this paper we report a high-resolution electron microscopy study of that $n = 1$ member of the series $Sr_2(Nd,Ce)_nNbCu_2O_{6+2n-\delta}$. The structure of $Sr_2NdNbCu_2O_8$ is determined and the defects present in this material are analyzed.

Experimental

$Sr_2NdNbCu_2O_8$ was prepared by solid state reaction of dried Nd_2O_3, $SrCO_3$, CuO, and Nb_2O_5 in the appropriate ratio. The best phase purity was obtained for successive overnight firings at 1050, 1125, and 1150° C in O_2 with intermediate grindings. The X-ray diffraction pattern was indexable on a simple tetragonal cell of $a = 0.39$ and $c = 1.17$ nm.

Thin specimens for electron microscopy were obtained by crushing or ion milling. The sample of $Sr_2NdNbCu_2O_8$ as prepared above and $Sr_2NdNbCu_2O_8$ occurring as a second phase in $Sr_2Nd_{1.5}Ce_{0.5}NbCu_2O_{10-\delta}$ (*4*) were investigated with electron microscopy. The defects presented in this paper occurred in both samples and were easy to find, indicating a fairly large density. Electron microscopy was performed with a Philips CM30ST electron microscope operating at 300 kV and equipped with side-entry 25°/25° tilt specimen holder and a Link EDX element analysis system.

The HREM images were recorded at a series of defocus values, and in particular at a defocus of about −40 nm at which all cations in [110] images are imaged as dark dots or at a defocus of about −80 nm where the cations are imaged as bright dots in [110] images. Image calculations have been carried out using a MacTempas software program, in which the following parameters were used: spherical aberation Cs is 1.2 mm, defocus spread is 9 nm, objective aperture is 6.5 nm^{-1}, beam convergence is 1.2 mrad, and mechanical vibration is 0.05 nm. The thickness and defocus varied.

A number of experimental HREM images were averaged over a number of unit cells to improve the ability to measure the gray values of the various positions. Images were digitized with about 50 pixels per nanometer. These images were noise reduced by first averaging each pixel over itself and its eight neighbors and then by averaging the image over a number of unit cells.

Experimental Results

Electron diffraction was carried out with a number of crystals, which were rotated to scan the reciprocal space. Electron diffraction patterns of the [100], [110], [210], and [001] orientations are given in Fig. 1. Superreflections indicating a tetragonal $a_p\sqrt{2}, a_p\sqrt{2}, c$ superstructure (a_p is the a-axis of a simple cubic perovskite) can be observed in the [210] and [001] diffraction patterns, leading to an unit cell of $a = b = 0.549$ and $c = 1.166$ nm. The absence of the superreflections in the [100] patterns show the reflections $(h0l)$ with $h \neq 2n$ to be systematically absent, indicating the space group to be $P4bm$. The superreflections are mostly streaked along the c^* axis (as in Fig. 1d) indicating that the ordering of the superstructure along the c-axis is weak. The strongest intensities in the streaks occur at the positions (hkl) with $l = n$ (consistent with space group $P4bm$), but also increased intensities can be observed at the positions

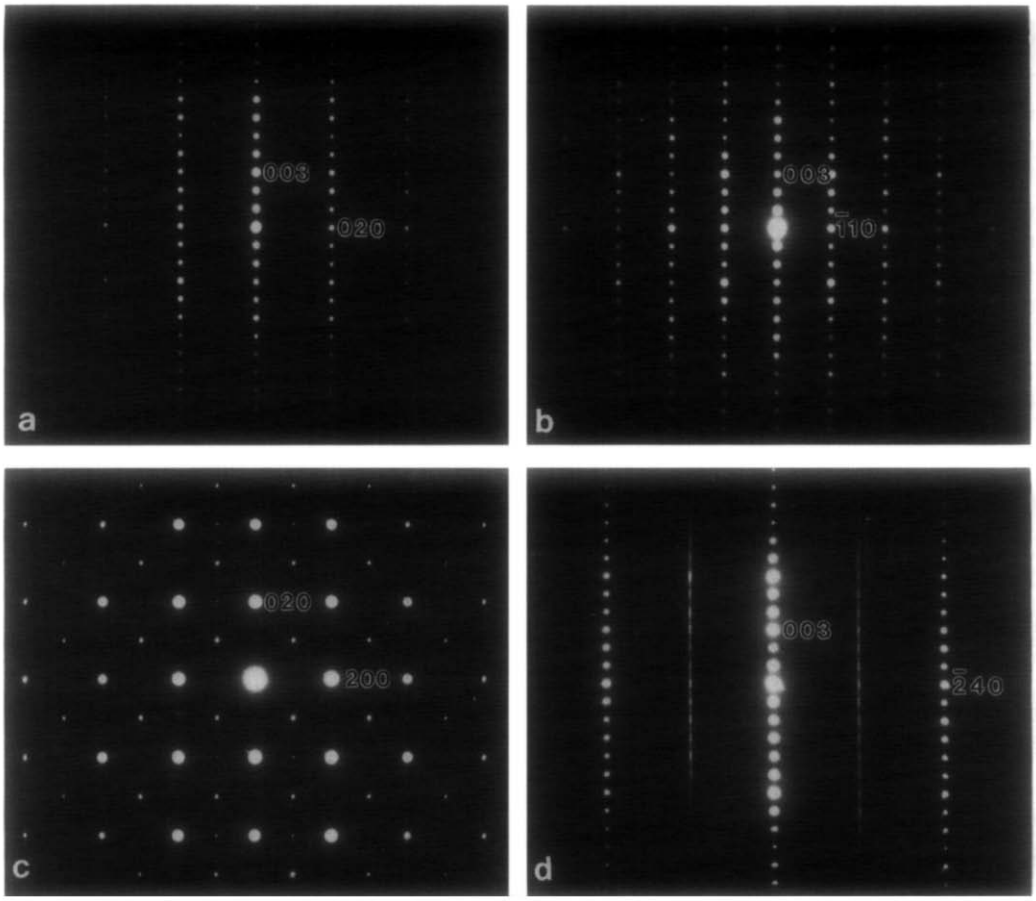

FIG. 1. Electron diffraction patterns along (a) [100], (b) [110], (c) [001], and (d) [210]. Note the streaking in (d) with increased intensities in these streaks at the positions $\{hkl\}$ with $l = n$ and $l = n + \frac{1}{2}$.

(hkl) with $l = n + \frac{1}{2}$, indicating that a part of the superstructure ordering is I-centered rather than primitive.

HREM was performed to determine the structure of $Sr_2NdNbCu_2O_8$. The observed [110] images reveal the stacking of the various layers because all cations can be imaged as individual dark dots (Fig. 2). Image calculations have been carried out with a model (see Fig. 3) based on the structure of $Sr_2Nd_2TaCu_2O_{10}$ reported by Li *et al.* (*5*), in which one O_2 layer and a Nd layer have been taken out with a subsequent reduction in the c-axis to 1.166 nm. The calculated images show good agreement with the experimental images, an example of which is given in Fig. 2. Similarly, the agreement between experimental and calculated [100] images is good.

The $a_p\sqrt{2}, a_p\sqrt{2}, c$ superstructure is also visible in [210] HREM images (see Fig. 4). The superstructure features of $Sr_2NdNbCu_2O_8$ are identical to those in $Sr_2Nd_{1.5}Ce_{0.5}NbCu_2O_{10-\partial}$ (*4*). Detailed analysis of the latter compound (*4*) showed that the superstructure is caused by tilting of the NbO_6 octahedra.

Three types of defects were observed: (i) intergrowths of a phase with a simple perov-

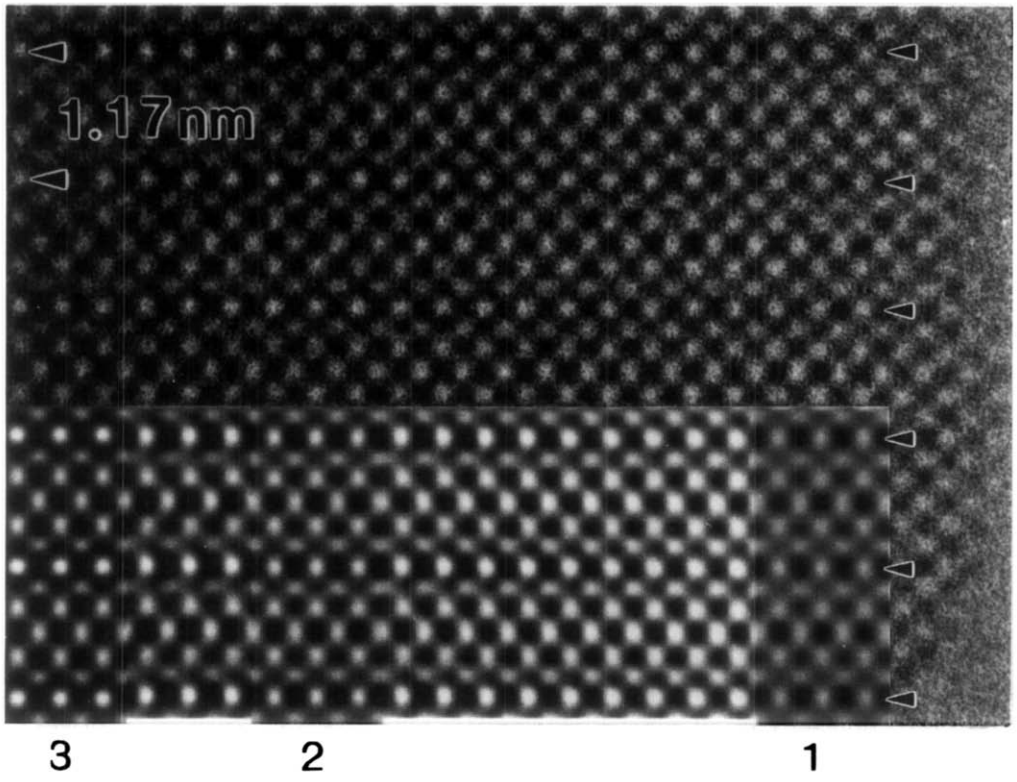

FIG. 2. A [110] micrograph taken at a defocus value of about −40 nm. In the lower part of the image the experimental image averaged over 4 and 8 unit cells along the [−110] and [001] directions, respectively, is given. Insets in the lower part of the image show calculated images labeled 3, 2, and 1 for a defocus value of −40 nm and a thickness of 3, 2, and 1 nm, respectively. The planes with the Nd atoms (imaged as black dots) are indicated by arrows.

skite structure, (ii) edge dislocations, and (iii) [100] 90° rotation twins.

An example of the first defect is shown in Fig. 5, and it is observed in many of the crystal fragments investigated. Figure 5 shows a perovskite-like intergrowth viewed along [110]. The $a_p\sqrt{2}, a_p\sqrt{2}$ superstructure in this intergrowth can mostly be observed in [210] images but it is considerably weaker than that in the matrix material. EDX analysis of these intergrowths was not possible. EDX analyses of similar and somewhat larger intergrowths in $Sr_2Nd_{1.5}Ce_{0.5}NbCu_2O_{10-\delta}$ (*4*) indicate a composition of $SrNb_{1-x}Cu_xO_y$, with x being 0.25(10). This composition is similar to a perovskite-like second phase, which was found to be present in $Sr_2NdNbCu_2O_8$ with a composition of approximately $Sr_{0.89}Nd_{0.11}Nb_{0.65}Cu_{0.35}O_x$.

An example of an edge dislocation is shown in Fig. 6. In this figure an extra 0.39-nm unit ends at the dislocation, leading to an edge dislocation with a Burgers vector of **a**/2-**b**/2[110].

Figure 7 shows a HREM image of a [110] 90° rotation twin. The twin planes are parallel to (001). This type of twin is observed regularly. They were observed more often in $Sr_2NdNbCu_2O_8$ when present as a second phase in a sample of $Sr_2Nd_{1.5}Ce_{0.5}NbCu_2O_{10-\delta}$. Because $Sr_2NdNbCu_2O_8$, when present as a second phase, did not contain

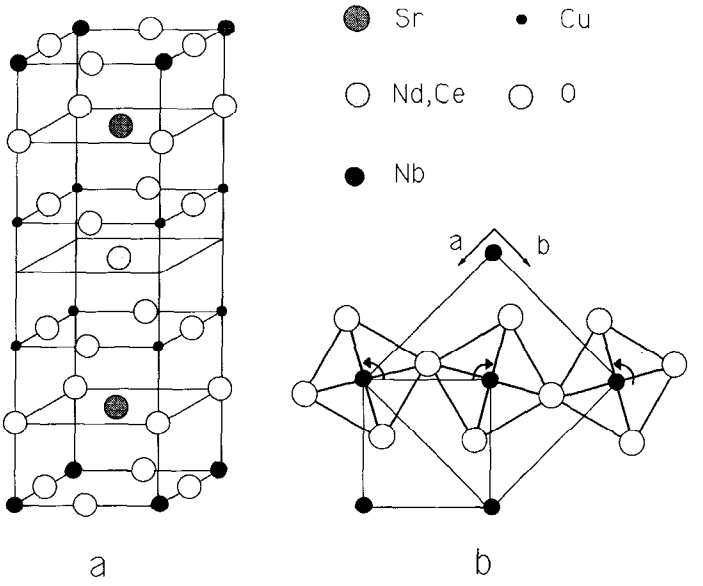

FIG. 3. Schematic representation of (a) the basic structure of $Sr_2NdNbCu_2O_8$ and (b) a NbO_2 plane in (001) projection with the coupled tilts of the NbO_6 octahedra.

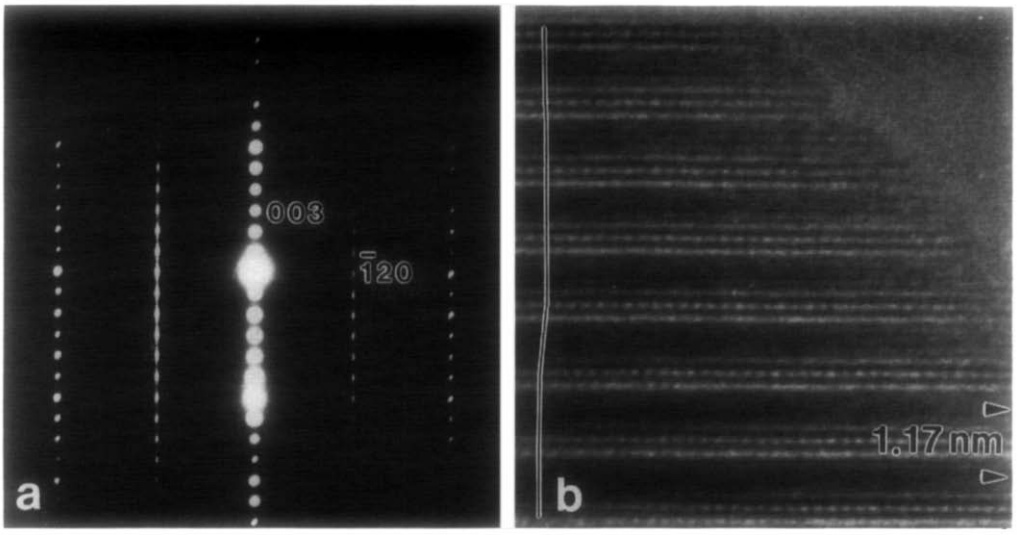

FIG. 4. A [210] diffraction pattern and HREM image showing the superstructure, which is due to tilts of the NbO_6 octahedra. The white dots in the HREM image are located on the NbO_2 plane. The line drawn in an (almost) vertical direction indicates the stacking of the superstructure, which is primitive except for one stacking.

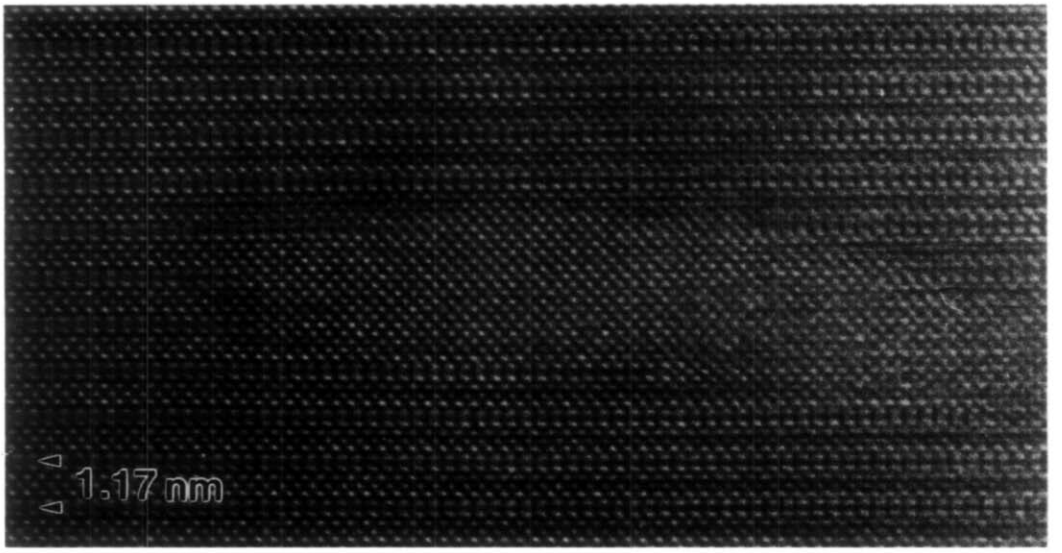

FIG. 5. A [110] micrograph recorded at a defocus value of about −80 nm showing an $Sr(Nb,Cu)O_3$ intergrowth in $Sr_2NdNbCu_2O_8$.

a significant amount of Ce, the Ce/Nd ratio cannot be the cause of the difference in occurrence of these [110] 90° rotation twins. This difference in occurrence is probably caused by differences in the preparation conditions, which are 1150 °C and 2 atm of oxygen in this case and 1125 °C and 25 atm in the Nd–Ce case.

Discussion and Conclusions

The structure of $Sr_2NdNbCu_2O_8$ consists of a layer sequence Nd–CuO_2–SrO–NbO_2–SrO–CuO_2 having a perovskite-like structure. The structure is very similar to the structure of $YBa_2Cu_3O_{7-\delta}$: Y is replaced by Nd and the $CuO_{1-\delta}$ layer is replaced by a NbO_2 layer. The superstructure is caused by rotations of the NbO_6 octahedra about the *c*-axis.

The structure of $Sr_2NdNbCu_2O_8$ is related to that of $Ba_2La(NbCu_2)O_8$ (*6*). The latter compound also has an $a_p\sqrt{2}, a_p\sqrt{2}$ superstructure. Rey *et al.* (*6*) suggest space group *I*4*cm* as the most probable space group of the superstructure of $Ba_2La(NbCu_2)O_8$; this requires a doubling of the *c*-axis. Electron diffraction on $Sr_2NdNbCu_2O_8$ shows that the stacking of the superstructure along the *a*-axis is predominantly primitive in symmetry, leading to the space group *P*4*bm*. But some *I*-centered stacking and random stacking are also present as is evident from the [210] diffraction patterns. We note that, up to the present time, neither $Ba_2La(NbCu_2)O_8$ nor $Sr_2NdNbCu_2O_8$ has successfully been made superconducting.

$Sr_2NdNbCu_2O_8$ is a potential superconductor. The most plausible kinds of hole doping can be done by substitution of Nd^{3+} by Ca^{2+}, or of Nb^{5+} by a cation with a lesser valence. Doping by replacing Nd by Ca was found to be impossible, but the presence of Cu in $Sr(Nb,Cu)O_3$ indicates that Nb in $Sr_2NdNbCu_2O_8$ can be partly replaced by Cu. Further doping experiments are in progress.

HREM experiments on $Sr_2Nd_{1.5}Ce_{0.5}NbCu_2O_{10-\delta}$ show frequently the existence of defects which can be described with the se-

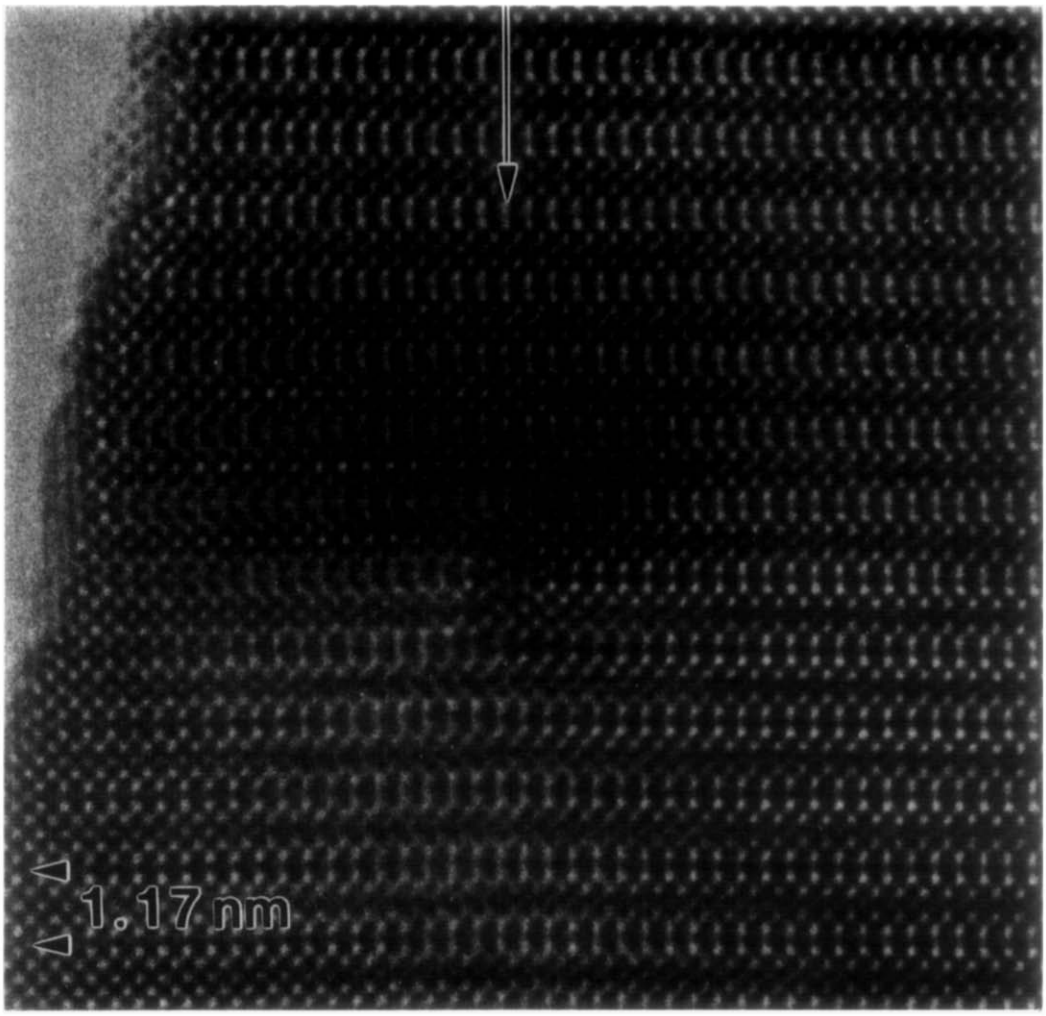

FIG. 6. A [110] micrograph recorded at about −40 nm showing an edge dislocation with a Burgers vector **a**/2-**b**/2 [110]. The extra lattice plane ending at the dislocation is indicated with an arrow. The region around the dislocation is strained, leading to strong changes in contrast and to local loss of symmetry in the image.

ries $Sr_2(Nd,Ce)_nNbCu_2O_{8+2n-\delta}$ (n = 1, 2, 3, 4, 5). Also for the compound $(Ce,Y)_3Sr_2Cu_2(Cu,Fe)O_{11}$ (*4*, *5*) such a series of defects is reported (*7*, *8*). However, such defects do not occur at all in $Sr_2NdNbCu_2O_8$. This is probably caused by the absence of Ce^{4+} which will stabilize the phase with larger values of n. We have not yet been able to prepare materials with $n > 2$ as bulk phases.

The lowering of the symmetry due to the superstructure is related to the rotation of the NbO_6 octahedra. As mentioned in previous papers this leads to a situation in which all atoms except for the oxygen ions in the NbO_2 layer still adopt the basic tetragonal unit cell with $a = b = 0.388$ nm. The deviation of these oxygen positions from the basic structure can be described as a perturbation. In this way the structure can be described

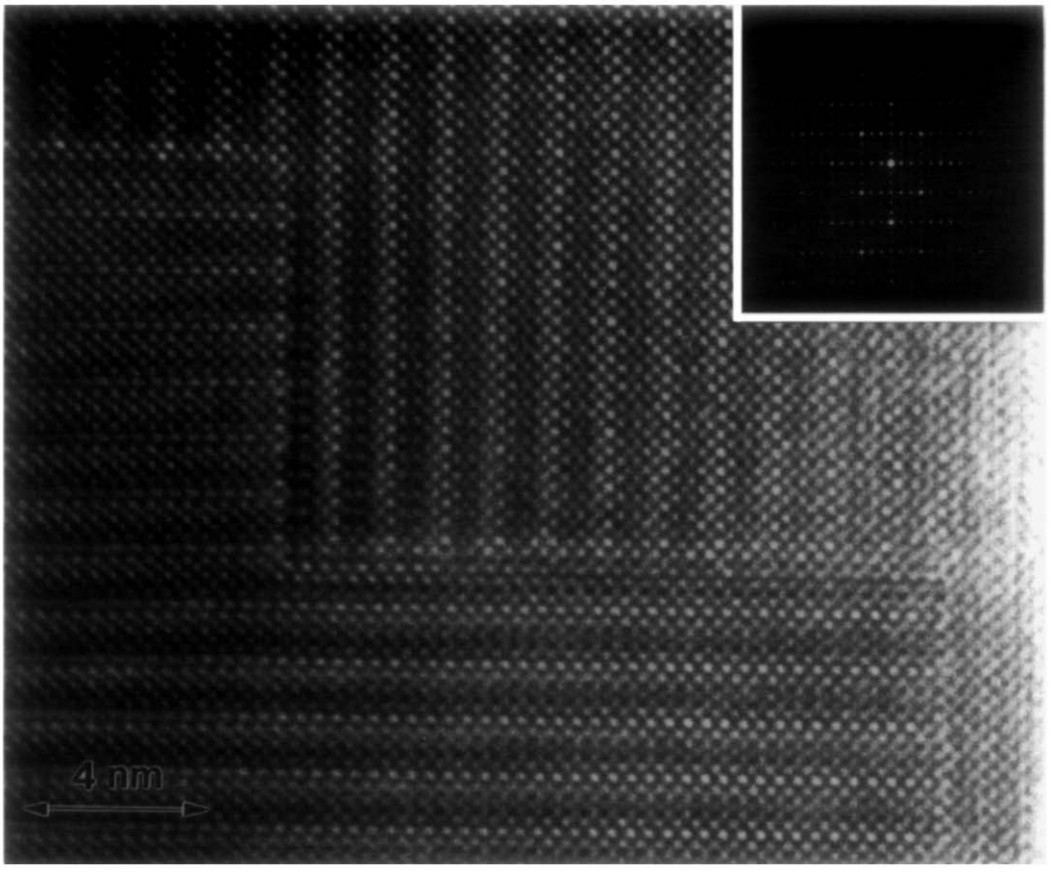

FIG. 7. A [110] micrograph taken at a defocus value of about −80 nm showing a [110] 90° rotation twin. The absence of strain at the twin boundaries indicates that the length of the *c* axis is almost three times d_{110}. The diffraction pattern is given in the top right corner.

with a four-dimensional space group (*9*), which allows more symmetry to be retained. Research is in progress to describe the superstructure of all phases in the series $Sr_2(Nd,Ce)_nNbCu_2O_{8+2n-\delta}$ (n = 1, 2, 3, 4, 5) with one four-dimensional space group.

The [100] 90° rotation twins were found to be dependent on the preparation conditions. These twins will only be formed when the c/a ratio is very close to 3, since otherwise too much stress will be induced by the lattice mismatch. A clear correlation between the c/a ratio and the density of [100] 90° rotation twins is reported for $YBa_2Cu_3O_{7-\delta}$ (*10*), where it is shown that the density of these twins is high only if the c/a ratio is close to 3.

References

1. J. G. BEDNORZ AND K. H. MÜLLER, *Z. Phys.* **B64,** 189 (1986).
2. R. J. CAVA, J. J. KRAJEWSKI, H. TAKAGI, H. W. ZANDBERGEN, R. B. VAN DOVER, W. F. PECK, JR., AND B. HESSEN, *Physica C* **191,** 237 (1992).
3. H. W. ZANDBERGEN, R. J. CAVA, J. J. KRAJEWSKI, AND W. F. PECK, JR., *Physica C* **192,** 223 (1992).
4. H. W. ZANDBERGEN, R. J. CAVA, J. J. KRAJEWSKI, AND W. F. PECK, JR., *Physica C* **196,** 252 (1992).
5. R. K. LI, Y. J. ZHU, Y. T. QIAN, AND Z. Y. CHEN, *Physica C* **176,** 19 (1991).
6. M.-J. REY, PH. DEHAUDT, J. JOUBERT, AND A. W. HEWAT, *Physica C* **167,** 162 (1990).

7. H. W. ZANDBERGEN, T. WADA, A. NARA, H. YAMAUCHI, AND S. TANAKA, *Physica C* **183,** 149 (1991).
8. A. TOKIWA, T. OKU, M. NAGOSHI, AND Y. SYONO, *Physica C* **181,** 331 (1991).
9. P. M. DE WOLFF, T. JANSSEN, AND A. JANNER, *Acta Cryst.* **A37,** 625 (1981).
10. H. W. ZANDBERGEN, R. GRONSKY, M. Y. CHU, L. C. DEJONGHE, G. F. HOLLAND, AND A. STACY, *Physica C* **166,** 255 (1990).